Eur Biophys J (1994) 22:423–436

European Biophysics Journal

Molecular dynamics simulation of a phospholipid membrane

Egbert Egberts*, Siewert-Jan Marrink, Herman J. C. Berendsen

Department of Biophysical Chemistry, University of Groningen, Nijenborgh 4, 9747 AG Groningen, The Netherlands

Received: 19 May 1993 / Accepted in revised form: 14 September 1993

Abstract. We present the results of molecular dynamics (MD) simulations of a phospholipid membrane in water, including full atomic detail. The goal of the simulations was twofold: first we wanted to set up a simulation system which is able to reproduce experimental results and can serve as a model membrane in future simulations. This goal being reached it is then further possible to gain insight in to those properties that are experimentally more difficult to access. The system studied is dipalmitoylphosphatidylcholine/water, consisting of 5408 atoms. Using original force field parameters the membrane turned out to approach a gel-like state. With slight changes of the parameters, the system adopted a liquid-crystalline state. Separate 80 ps runs were performed on both the gel and liquid-crystalline systems. Comparison of MD results with reliable experimental data (bilayer repeat distance, surface area per lipid, tail order parameters, atom distributions) showed that our simulations, especially the one in the liquid-crystalline phase, can serve as a realistic model for a phospholipid membrane. Further analysis of the trajectories revealed valuable information on various properties. In the liquid-crystalline phase, the interface turns out to be quite diffuse, with water molecules penetrating into the bilayer to the position of the carbonyl groups. The 10–90% width of the interface turns out to be 1.3 nm and the width of the hydrocarbon interior 3.0 nm. The headgroup dipoles are oriented at a small angle with respect to the bilayer plane. The resulting charge distribution is almost completely cancelled by the water molecules. The electron density distribution shows a large dip in the middle of the membrane. In this part the tails are more flexible. The mean life time between dihedral transitions is 20 ps. The average number of gauche angles per tail is 3.5. The occurrence of kinks is not a significant feature.

* *Present address:* Philips Research Laboratories, P.O. Box 80000, 5600 JA Eindhoven, The Netherlands

Abbreviations: MD, molecular dynamics; DPPC, dipalmitoylphosphatidylcholine; SPC, simple point charges; DPPE, dipalmitoylphosphatidylethanolamine

Correspondence to: H. J. C. Berendsen

Key words: Computer simulation – DPPC – Bilayer – Liquid crystalline

Introduction

We have previously reported molecular dynamics (MD) simulations of simple bilayer membrane models without solvent (van der Ploeg and Berendsen 1982, 1983) and of a smectic liquid crystal, consisting of a ternary system of water and simple alcoholic and fatty acid components (Egberts 1988; Egberts and Berendsen 1988). These systems served as relatively primitive and purely artificial models of a biological membrane.

Increasing computer power allowed us to replace the simple model by a more sophisticated one. We chose the binary system dipalmitoylphosphatidylcholine (DPPC)/water as representative for a biological membrane, which consists mainly of phospholipids. The structural formula is given in Fig. 1. The parafinic chains are fully saturated and of equal length (16 carbon atoms). The lecithin headgroup is a zwitterion, overall neutral, with a charge $+e$ distributed over the choline group and a charge $-e$ on the phosphate group. We simulated the biologically relevant L-enantiomer.

There is an overwhelming amount of experimental data on lecithin/water systems. These comprise data on lecithin-containing natural membranes and on membranes formed by lecithins extracted from egg-yolk or synthetic lecithins. The experiments cover the entire phase diagram of lecithin/water systems and give information on molecular conformations, order parameters, diffusion, hydration and so forth. Experimental techniques employed range from differential scanning calorimetry and thermal analysis, X-ray and neutron scattering to spectroscopic methods (NMR, ESR, infrared and Raman spectroscopy). We shall compare MD results with experimental data whenever possible.

Theoretical treatments of lipid/water systems will suffer from a lack of rigor or a lack of realism as the complex-

ity of the system makes more or less crude assumptions necessary. This oversimplification makes it difficult to compare these treatments with our approach, the accuracy of which at the atomic level is restricted only by the accuracy of the forcefield used. Sometimes, however, theoretical calculations give additional insight and will be used to interpret the MD results.

We will also compare the results of our new simulations with our previous simulations as well as some other recent simulations of lipid systems. In general, the MD technique is a highly valuable instrument for obtaining structural and dynamical information on systems as complicated as lipid/water dispersions. Whereas theoretical approaches lose their power owing to oversimplifying assumptions, and experimental results may scatter widely and are often difficult to interpret on an atomic level, the MD method yields trajectories, the interpretation of which is straightforward. Moreover, MD can address relevant details which are experimentally inaccessible.

In the next section the technical details of the simulation method as well as the composition and parametrization of the lecithin/water system will be given, followed by a description of the set up of the system and the extensive equilibration procedure. Then the description and discussion of the results of two separate 80 picosecond MD runs are presented, one with the membrane approaching the gel phase and the other with the membrane in the liquid-crystalline phase. Finally, some conclusions are drawn.

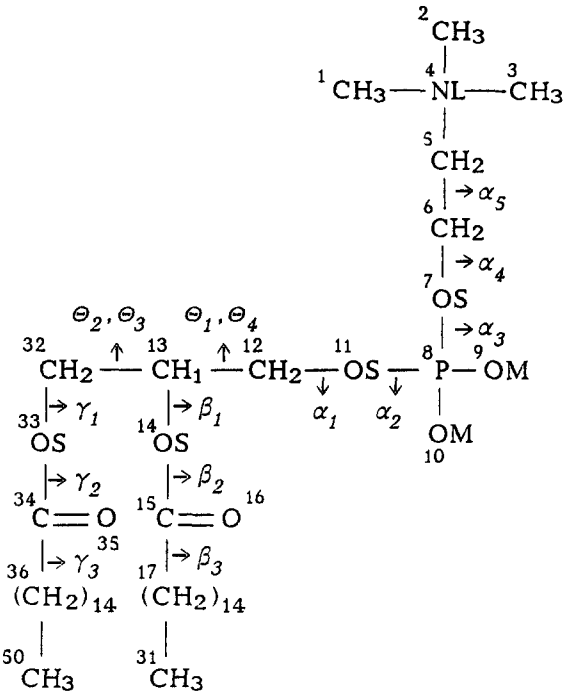

Fig. 1. Structural formula of dipalmitoylphosphatidylcholine (DPPC), with numbering of atoms and atom groups and indication of dihedral angles. GROMOS symbols are used for atoms: NL = Nitrogen, OS = Ester Oxygen, OM = Phosphate Oxygen, O = Carbonyl Oxygen

Method and model

Simulation method

The computational unit cell contained a bilayer of 64 DPPC molecules and a water layer of 736 molecules, which amounts to 5408 atoms. Periodic boundary conditions were applied in all three dimensions, so that the simulation is actually that of a multilamellar system. In the molecular dynamics simulation method atomic trajectories are calculated through numerical integration of Newton's equations of motion. We applied a leap-frog algorithm (Hockney and Eastwood 1981) to solve the equations. The integration time step was set to 2 fs. Bond lengths were constrained by the SHAKE method (Ryckaert et al. 1977; van Gunsteren and Berendsen 1977). A cut-off radius for Lennard-Jones interactions of 0.75 nm was used. For Coulomb interactions an extra long-range term was calculated over a cylindrical volume with a cut-off radius of 1.7 nm every tenth time step. The types of intra- and intermolecular interactions used in the algorithm are described below.

The system was weakly coupled to a temperature bath (Berendsen et al. 1984). Independent scaling of the velocities of solute and solvent molecules was performed, both with a coupling time constant of 0.1 ps. The system was kept at an isotropic pressure of 1 atmosphere by a weak coupling to a pressure bath (Berendsen et al. 1984). The three unit cell dimensions were scaled independently, with a coupling time constant of 0.5 ps.

The simulation program that was used is based on GROMOS (van Gunsteren and Berendsen 1987). The program was adapted for more efficient use in the simulation of a lecithin membrane, resulting in a performance of 1 ps simulation (500 steps) per 2.5 h CPU time on a Cyber 170/760. It was not feasible to perform more than a small part of the runs (taking typically 200 ps, including equilibration) on the multi-user system. Therefore, the program was extensively vectorized for use on a Cyber 205 computer. A speed of 3.5 ps simulation per hour CPU time on a one-pipe Cyber 205 machine could be realized.

Model parameters

The lecithin molecules are treated in full atomic detail with the exception of CH, CH_2 and CH_3 groups that are treated as single Lennard-Jones centers (united atoms). The water molecules were modelled as simple point charges (SPC) (Berendsen et al. 1981). For Lennard-Jones interactions the H_2O molecule is treated as a united atom centered on the oxygen atom.

The parameters ultimately used in the simulations are listed in Tables 1 to 5.

Setup and equilibration

Setup of the starting configuration

The contents of the simulation unit cell corresponds to exactly 11.5 water molecules per lecithin molecule or

Table 1. Lennard-Jones parameters ε_{ij} (kJ/mol, upper values) and σ_{ij} (nm, lower values)[a]

	NL	O	OM	OS	P	C	CH_1	CH_2	CH_3	OW
A) Normal interactions[b]:										
OW	0.320	0.811	0.495	0.743	1.261	0.968	1.121	0.997	1.201	0.650
	0.354	0.301	0.327	0.306	0.327	0.294	0.329	0.310	0.310	0.317
CH_3	0.741	1.038	1.038	1.038	1.237	0.504	0.583	0.519	0.625	
	0.333	0.313	0.313	0.313	0.356	0.355	0.398	0.374	0.374	
CH_2	0.620	0.862	0.862	0.862	1.026	0.418	0.477	0.430		
	0.333	0.313	0.313	0.313	0.356	0.355	0.399	0.374		
CH_1	0.691	0.969	0.969	0.969	1.154	0.470	0.544			
	0.355	0.333	0.333	0.333	0.378	0.377	0.423			
C	0.597	0.837	0.837	0.837	0.997	0.406				
	0.316	0.297	0.297	0.297	0.337	0.336				
P	1.464	1.527	0.577	1.441	2.446					
	0.317	0.312	0.368	0.316	0.399					
OS	0.366	1.725	1.725	1.725						
	0.342	0.263	0.263	0.263						
OM	0.146	1.725	1.725							
	0.399	0.263	0.263							
O	0.399	1.725								
	0.337	0.263								
NL	0.877									
	0.298									
B) 1–4 interactions[b]:										
OW	1.423	1.996	1.996	1.996	2.376	0.968	1.144	1.345	1.498	2.310
	0.276	0.259	0.259	0.259	0.295	0.294	0.291	0.295	0.298	0.256
CH_3	0.924	1.295	1.295	1.295	1.543	0.628	0.743	0.874	0.973	
	0.322	0.302	0.302	0.302	0.343	0.342	0.338	0.343	0.347	
CH_2	0.829	1.163	1.163	1.163	1.385	0.564	0.667	0.784		
	0.317	0.298	0.298	0.298	0.339	0.337	0.334	0.339		
CH_1	0.705	0.989	0.989	0.989	1.179	0.480	0.567			
	0.313	0.294	0.294	0.294	0.334	0.333	0.323			
C	0.597	0.837	0.837	0.837	0.997	0.406				
	0.316	0.297	0.297	0.297	0.337	0.336				
P	1.464	2.055	2.054	2.054	2.446					
	0.317	0.298	0.298	0.298	0.399					
OS	1.229	1.725	1.725	1.725						
	0.280	0.263	0.263	0.263						
OM	1.229	1.725	1.725							
	0.280	0.263	0.263							
O	1.229	1.725								
	0.280	0.263								
NL	0.877									
	0.298									

[a] Lennard-Jones potential: $V(r_{ij}) = 4\,\varepsilon_{ij}\,((\sigma_{ij}/r_{ij})^{12} - (\sigma_{ij}/r_{ij})^{6})$

[b] Lennard-Jones 1–4 interactions have different values of ε_{ij} and σ_{ij}. Lennard-Jones interactions are excluded for nearest and next-nearest neighbours, as well as for 1–4 interactions of groups that are treated by the Ryckaert-Bellemans potential

Table 2. Equilibrium bond lengths (nm)[a]

$NL-CH_n$	0.147	CH_n-OS	0.143	$C-CH_2$	0.153
P–OM	0.148	C–OS	0.136	CH_n-CH_n	0.153
P–OS	0.161	C=O	0.123	OW–HW	0.100

[a] Bond lengths are constrained by the SHAKE method (van Gunsteren and Berendsen 1977; Ryckaert et al. 1977)

22% water by weight. From the phase diagram of the DPPC/water system, which is by now well established (e.g. Chapman et al. 1967; Tardieu et al. 1973; Janiak et al. 1976, 1979; Ulmius et al. 1977) we infer that this composition should be in the biologically interesting liquid-crystalline phase (L_α) for temperatures above the main phase transition at 315 K.

Table 3. Equilibrium bond angles and force constants[a]

	k_α (kJ mol^{-1} rad^{-2})	α_0 (degrees)
$CH_n-NL-CH_n$	460	109.5
$NL-CH_2-CH_2$	460	109.5
CH_2-CH_n-OS	460	109.5
$P-OS-CH_2$	397	120.0
$OS-P-OM$	397	109.6
$OS-P-OS$	397	103.0
$OM-P-OM$	585	120.0
$OS-CH_2-CH_1$	460	111.0
$CH_2-CH_2-CH_n$	460	111.0
$CH_2-CH_1-CH_2$	460	109.5
CH_n-OS-C	418	120.0
$OS-C=O$	502	124.0
$OS-C-CH_2$	502	115.0
$O=C-CH_2$	502	121.0
$C-CH_2-CH_2$	585	120.0

[a] Angle potential: $V(\alpha)=1/2\, k_\alpha(\alpha-\alpha_0)^2$

Table 4. Parameters for dihedral interactions[a]

	C (kJ/mol)	n	δ (degrees)
A) Proper dihedrals[b]			
$CH_3-NL-CH_2-CH_2$	3.76	3	0.0
$NL-CH_2-CH_2-OS$	5.85	3	0.0
CH_2-CH_2-OS-P	3.76	3	0.0
$CH_2-OS-P-OS$	1.05	3	0.0
$CH_2-OS-P-OS$	3.14	2	0.0
CH_1-CH_2-OS-P	3.76	3	0.0
$OS-CH_1-CH_2-CH_1$	5.85	3	0.0
$OS-CH_1-CH_2-CH_1$	0.42	2	0.0
$OS-CH_1-CH_2-OS$	2.09	2	0.0
CH_2-CH_1-OS-C	3.77	3	0.0
$OS-C-CH_2-CH_2$	0.42	6	0.0
CH_1-CH_2-OS-C	3.76	3	0.0
$C-CH_2-CH_2-CH_2$	5.86	3	0.0
$CH_n-OS-C-CH_2$	16.74	2	180.0

	C (kJ/mol)	α_0 (degrees)
B) Improper dihedrals[c]		
$CH_1-OS-CH_2-CH_2$	335.0	35.264
$C-OS-CH_2-O$	167.0	0.0

[a] For the tail group dihedrals $CH_2-CH_2-CH_2-CH_n$ we used the Ryckaert-Bellemans potential (Ryckaert and Bellemans 1975, 1978)
[b] Normal dihedral potential: $V(\varphi)=C(1+\cos(n\varphi-\delta))$
[c] Improper dihedral potential: $V(\alpha)=1/2\, C(\alpha-\alpha_0)^2$

Table 5. Partial charges of atoms[a]

Choline group		Phosphate group		Glycerol linkage		Water	
$CH_3(3)$	0.248	OS(2)	−0.36	CH_1/CH_2	0.2	OW	−0.820
CH_2	0.248	OM(2)	−0.635	OS	−0.36	HW	0.410
NL	0.008	P	0.99	C	0.54		
				O	−0.38		

[a] Charges were derived from the quantum mechanical charge distribution. In the run with the reduced charges all the above partial atomic charges, except for the water, were reduced by a factor of 2

In order to set up an initial configuration for the system it is imperative to know both the surface area per headgroup of a lecithin (S) and the bilayer repeat distance (d) at the simulation temperature, which was set to 335 K. Various experiments (Chapman et al. 1967; Reiss-Husson 1967; Phillips et al. 1968; Levine and Wilkins 1971; Janiak et al. 1976, 1979; Büldt et al. 1979) on lecithin systems under similar conditions provide a substantial range of values. Taking average values, we conclude that $S=0.59$ nm^2 and $d=5.35$ nm are safe initial values, that give unit cell dimensions of 4.345 nm (x, y) and 5.35 nm (z). Note however that, simulating at constant pressure, the choice of initial values is not too critical. The volume of the box can adjust itself during the simulation.

Random configurations of DPPC molecules were generated with the help of program PROGCA in the GROMOS package. A bilayer of lecithins was formed from these conformations, allowing restricted rotations and out of plane displacements. An energy minimization of the single bilayer was performed. Water was added from a liquid SPC water configuration, followed by an energy minimization of the resulting DPPC/H_2O system, confined to a unit cell with the aforementioned dimensions.

Equilibration procedure

An equilibration run was started, with weak coupling of the system to a temperature bath of 335 K and to a pressure bath of 1 atmosphere. Increasing the masses of the SPC hydrogen atoms to 16 a.m.u. allowed a time step of 8 fs that coincides with the upper bound set by the dynamics of the hydrocarbon chains. After 120 ps another 40 ps run was performed with normal SPC water and a time step of 2 fs.

The x, y, and z unit cell dimensions stabilized at 3.975, 3.985, and 6.35 nm. Though these values imply a near perfect match with the experimental density, the bilayer repeat is 17% higher and the surface area per lecithin (0.495 nm^2) 17% lower than experimentally determined. These values are close to those obtained for lecithin/water systems in the tilted gel phase ($L_{\beta'}$) (Tardieu et al. 1973; Nagle and Wiener 1988). Therefore, we anticipated that the simulated system was in the gel phase at the present choice of interaction parameters and temperature. Curiosity led us to perform an 80 ps run on this system. During this run the lamellar repeat distance increased by another 2% to 6.50 nm. The x and y cell dimensions decreased to 3.96 nm and 3.92 nm, implying a surface area per lecithin molecule of 0.485 nm^2. The large value of the bilayer repeat distance makes the L_β phase a possible candidate. This phase is similar to the $L_{\beta'}$ phase except for the hydrocarbon chains which are perpendicular with respect to the bilayer plane instead of tilted over $\pm 30°$, so the bilayer repeat distance will be larger. Assuming that the tilt in the $L_{\beta'}$ phase refers to the first ten methyl groups of a hydrocarbon chain, with a length of 1.25 nm in an all-trans conformation, the bilayer thickness would increase by 0.35 nm on going from a tilted configuration to one with zero tilt. This would result in a value of d close to 6.5 nm.

Further analysis (see results and discussion) revealed that the system indeed shows the characteristics of this untilted gel phase. However, normal DPPC/water systems do not adopt a gel phase at all at the simulation temperature (335 K), let alone an untilted gel phase since the packing of the large headgroups results in too much free space between the hydrocarbon chains. To maximize the Vanderwaals attraction between the tails, they would adopt a tilted conformation. Therefore we assume that with the present choice of interaction parameters the attraction between the zwitterionic headgroups is overestimated, resulting in a stabilization of the gel phase above the liquid-crystalline phase and prohibiting the tilting of the chains. This is exactly the way in which DPPE, the ethanolamine analog of DPPC, behaves. Lacking the bulky methyl groups at the headgroups it is able to pack the headgroups closer together. As a result, an untilted gel phase is formed which remains stable until approximately 337 K (Cevc 1987). Another explanation for the lack of tilt is the absence of explicit hydrogen atoms in the methylene groups. Increasing evidence shows that the use of united atoms may influence the amount of tilt in lamellar systems (Moller et al. 1991; Bareman and Klein 1990; Chandrasekhar 1992).

Our goal, however, is the performance of a simulation of the system in the L_α phase. Short equilibration runs of the system with the same potential functions, but at elevated temperatures (375 K and 425 K) show an even faster increase of the bilayer repeat, and did not bring the system into the L_α phase. This may be explained by the fact that these temperatures are already close to and well above, respectively, the hexagonal phase transition temperature of the DPPE/water system at 392 K (Lewis et al. 1989). The range of temperatures over which the liquid-crystalline phase is stable for this system is quite narrow and therefore we tried another approach in order to reach the required phase. As in our previous simulation of a soap/alcohol/water system (Egberts 1988) and in the micelle simulation by Jönsson et al. (1986), we reduced the atomic charges on the lecithin molecule by a factor of two. The physical justification for this reparametrization is, in short, that the Coulomb interactions in the system are exaggerated owing to an insufficient screening performance of the SPC water molecules. In the simulation a dielectric constant of 1 is used while electronic polarization is neglected. We also changed the parameters for methyl and methylene groups and included the Ryckaert-Bellemans potential (Ryckaert and Bellemans 1975, 1978), which favors the appearance of gauche angles with respect to the GROMOS dihedral potential. The Ryckaert-Bellemans potential has proved to be more realistic for liquid alkanes. We expect that now the headgroup-headgroup attractions as well as the tail-tail interactions will be lower, allowing a lateral expansion and therefore destabilisation of the gel phase.

The equilibration run of the system with the revised forcefield at 350 K did stabilize after 80 ps, using increased hydrogen masses and a timestep of 8 fs. This equilibration was continued for another 40 ps, followed by 30 ps equilibration with normal SPC water and a time step of 2 fs. The unit cell dimensions along x, y, and z stabilized on 4.29, 4.29, and 5.61 nm. This implies a surface area per lecithin of 0.575 nm^2, which is very close to the expected experimental value (0.59 nm^2). The bilayer repeat is 5% higher than the experimental one. This is very reasonable, considering the spread in experimental data. An 80 ps run was consequently performed during which the unit cell dimensions showed only a minor drift to eventually attain values of 4.33, 4.35, and 5.64 nm along x, y, and z, respectively.

We thus have two 80 ps trajectories of the multilamellar DPPC/H_2O system, one in the L_α phase and one in the L_β phase. Although the L_α is of greater biological interest, most of the analyses have been performed on both of these trajectories.

Recent simulations of DPPC molecules (de Loof et al. 1991), using a combined approach of molecular and stochastic dynamics and a mean field, showed that only after several nanoseconds individual lipids had sampled their conformational space representatively. Therefore they expect that very long simulations are needed in order to reach full equilibrium. We do not expect that the motion of lipids on longer time scales (wobbling, rotation) will have a large effect on atom distributions, order parameters or dihedral transition rates. The random nature of the starting configuration used for the MD simulation assures largely independent statistics for the 64 lipid molecules during the simulation. This means that the statistics in one 80 ps run is equivalent to a 5 ns stochastic dynamics run on a single lipid molecule.

Results and discussion

Investigation of phase

In the previous section we claimed (based on cell dimensions) the system resulting from the simulation with full charges and GROMOS force field to be in the gel phase. This can be verified through the evaluation of the radial distribution function of the hydrocarbon tails of the lecithin molecules. It is well established that in the gel phase the chains pack in a (distorted) hexagonal lattice (Tardieu et al. 1973).

Tail vectors for palmitoyl chains were defined as the vectors connecting the middle of the C_2-C_3 bond with the middle of the $C_{11}-C_{12}$ bond in a chain, where C_1 is the carbonyl carbon. The intersections of these vectors with a plane $z=c$ were calculated, where c is the average z-coordinate of the bonds involved in the definition of the tail vectors. These intersection points, averaged over a few ps, are shown in Fig. 2a for the gel phase and in Fig. 2b for the liquid-crystalline phase. It is clear that in the gel phase domains exist where the packing of the chains is very close to hexagonal. These domains are separated by regions with a more random distribution of the chains and a lower chain density, which resembles the distribution in the liquid-crystalline phase. The formation of a complete hexagonal lattice will be very slow and is apparently not completed yet in the simulation.

The two-dimensional radial distribution function of the intersection points was calculated for both phases.

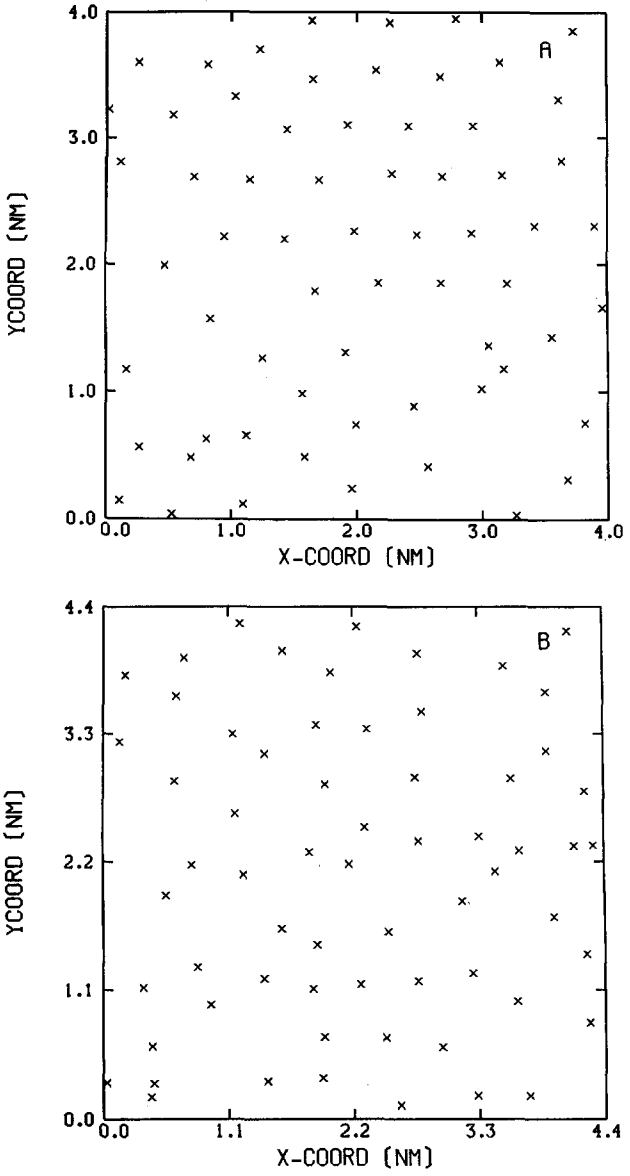

Fig. 2 A, B. Intersection points of palmitoyl tail vectors with a plane z = constant. Averaging over a few picoseconds in the simulation with physical charges **A** and with reduced charges **B**

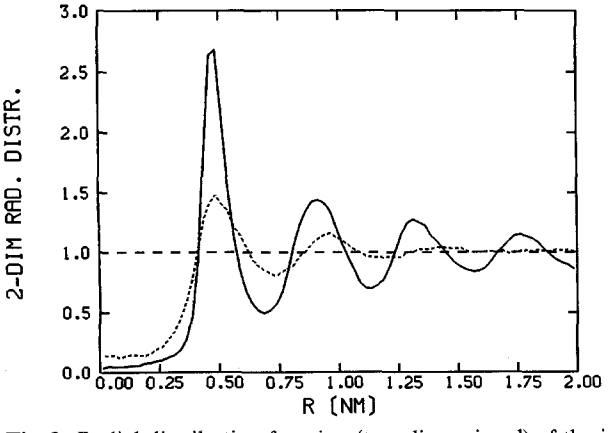

Fig. 3. Radial distribution function (two-dimensional) of the intersection points in Fig. 2, in the L_β (*solid line*) and in the L_α (*dashed line*) phase

This function is displayed in Fig. 3. In the L_β phase it is highly structured, with correlations extending over the unit cell, which is typical for a crystal. The counterpart for the L_α phase has a much broader and lower first order maximum, and no structure beyond the second order maximum.

From Fig. 3 the positions of the maxima for the L_β phase are found to be: 0.485, 0.915, 1.325, and 1.76 nm. In a purely hexagonal lattice with a separation of nearest neighbours of 0.485 nm, one expects resolved higher order maxima at 0.84/0.97, 1.28/1.45, and 1.69/1.75/1.94. The present distribution is not very sharp, and reflects features from both a hexagonal phase and a normal liquid phase. For the hexagonal region the surface area per tail is 0.204 nm^2, implying a surface area per lecithin of 0.408 nm^2. This value is very close to the reported value of 0.397 nm^2 for a (metastable) L_β phase of DPPC (Tenchov et al. 1987).

From the above arguments we conclude that the system simulated with full charges is partly in the gel phase. The formation of a complete gel phase will take much longer. The liquid-like regions can also be artifacts of the rectangular unit cell or result from a realistic phase separation when the system is just in the small two-phase region between the gel and liquid crystalline phase.

We verified that we have the untilted L_β phase instead of the tilted $L_{\beta'}$ phase. This can be shown by calculating the mean tilt angle of the tail vector which turns out to be close to 0°, whereas more than 30° is observed experimentally in the $L_{\beta'}$ phase (Tardieu et al. 1973; Nagle and Wiener 1988).

Distributions of atom types

Typical snapshots of the simulated system in the L_α phase are shown in Fig. 4. The time-averaged distributions of water molecules, nitrogen atoms, and phosphorous atoms are plotted in Fig. 5. From these figures it is clear that a diffuse interface exists, with water penetrating into the bilayer to a depth that corresponds to the position of the carbonyl group at the beginning of the palmitoyl tails. This is confirmed by neutron diffraction experiments (Büldt et al. 1979; Zaccai et al. 1980) which show that water penetrates up to 1.5 nm from the middle of the bilayer, near the acylester groups. The hydrocarbon interior of the membrane is devoid of water. Defining the interface as the region where the water concentration is between 10% and 90% of its maximum value, the width of the interface turns out to be 1.3 nm. From X-ray measurements (Inoko and Mitsui 1978; Lis et al. 1982; Ruocco and Shipley 1982) a similar value can be calculated (Nagle and Wiener 1988). Taking twice this value (both interfaces) this means that more than 40% of the total membrane belongs to the interfacial region. The width of the hydrocarbon interior of the membrane is then calculated to be 3.0 nm, which also agrees well with the X-ray results. A definition of the bilayer thickness as the P−P or N−N distance gives 4.0 and 4.4 nm, respectively. Neutron diffraction experiments (Büldt et al. 1978, 1979) give a distance of ± 4.35 nm between choline CH_3 groups and of

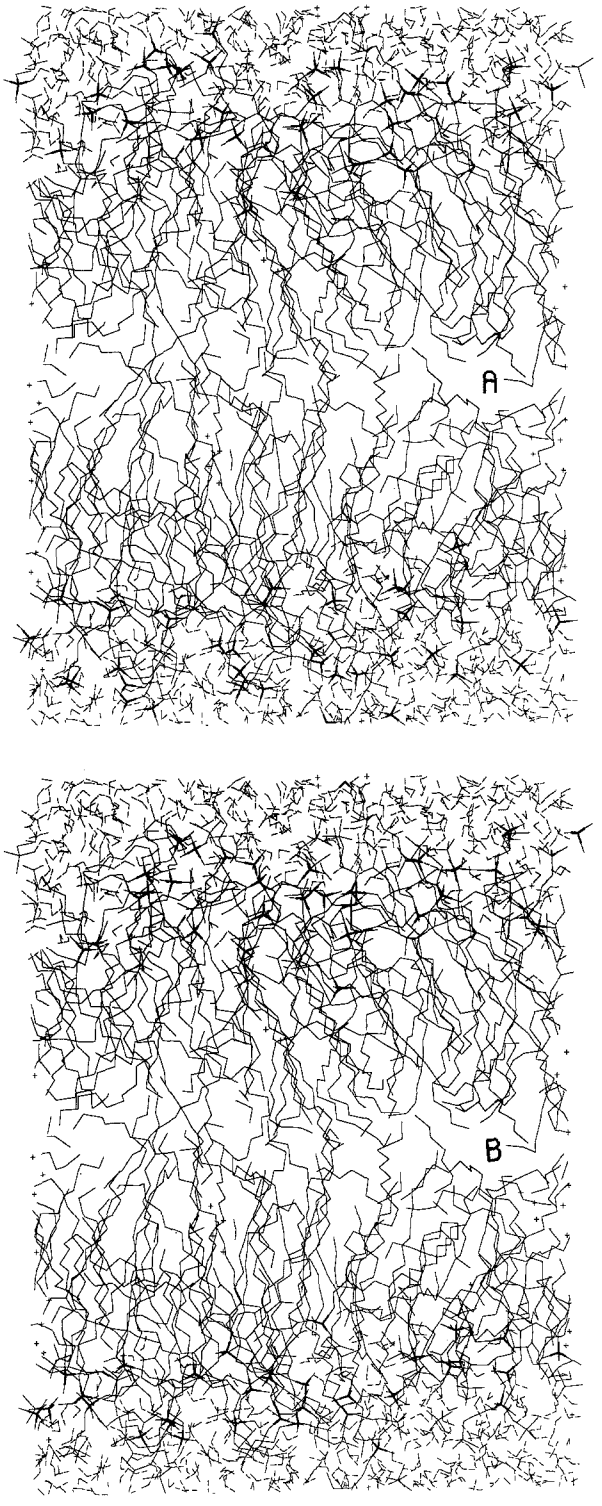

Fig. 4 A–C. Snapshots of the membrane in the L_α phase. *Bold lines* are used for choline groups **A**, phosphate groups **B** and carbonyl groups **C**. *Dashed lines* are used for the water molecules, *solid lines* for the other bonds

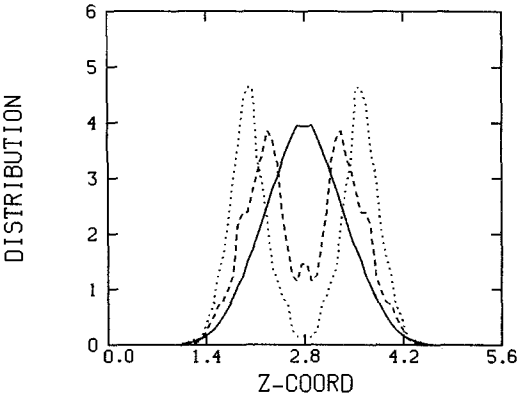

Fig. 5. Distributions along bilayer normal of water (*solid line*), nitrogen (*dashed line*), and phosphorus (*dotted line*) in the L_α phase. The middle of the bilayer corresponds with $z=0$, the middle of the water layer with $z=2.8$ nm

± 4.2 nm between choline CH_2 groups linked to the phosphate moiety. The value of 4.0 nm for the P–P distance obtained by X-ray experiments (Lewis and Engelman 1983) exactly matches our value. The broader distribution of the nitrogen atoms with respect to the phosphorous atoms can be explained by a greater mobility of the choline group or by rotations of the headgroup as a whole around the glycerol backbone. Combined X-ray and neutron diffraction experiments (Wiener and White 1992b) on dioleoylphosphatidylcholine were interpreted as Gaussian distributions for groups of atoms: the phosphate width (full width at half height) was 0.51 nm and the choline width was 0.58 nm. Our L_α simulation gives values of 0.53 and 0.66 nm, respectively.

Figure 6 gives the distributions of water, nitrogen and phosphorous in the L_β phase. The interface is markedly more diffuse in this case. A more pronounced penetration of water occurs although the percentage of water molecules that penetrate into the region of the palmitoyl tails is actually very small. The broad distributions of the water molecules and headgroup atoms might be due to

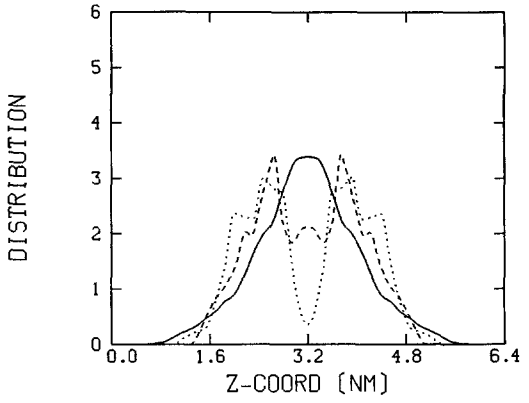

Fig. 6. Distributions along bilayer normal of water (*solid line*), nitrogen (*dashed line*), and phosphorus (*dotted line*) in the L_β phase. The middle of the bilayer corresponds with $z=0$, the middle of the water layer with $z=3.2$ nm

Table 6. Mean positions (nm) and half widths of tail carbon atoms[a]

	MD, L_α	EXP, L_α	MD, L_β	EXP, L_β
C_4	1.33±0.39	1.22±0.27	1.59±0.66	1.54±0.25
C_5	1.24±0.38	1.05±0.27	1.47±0.65	1.37±0.27
C_9	0.84±0.40	0.81±0.31	1.00±0.58	0.98±0.27
C_{12}	0.56±0.41	0.57±0.34	0.69±0.56	−±−
C_{14}	0.41±0.44	0.36±−	0.47±0.56	0.41±0.28
C_{15}	0.31±0.60	0.19±−	0.37±0.50	0.25±0.29

[a] All values are averaged over both tails. Some experimental half widths are extrapolations from other phases. The carbon atom C_4 corresponds with the carbon atoms 19 and 38 of Fig. 1

the presence of liquid-like regions. Packing defects on the boundary of the gel and liquid-like region allow a larger penetration of the water molecules and headgroup atoms. The bilayer width of 4.8 nm compares well with the values of 4.5 nm (Braganza and Worcester 1986) and 4.8 nm (Büldt et al. 1978, 1979) from neutron diffraction and with the values of 4.6 nm (Chapman et al. 1967) and 4.85 nm (Tardieu et al. 1973) from X-ray diffraction.

The mean z-positions and half widths of the distributions of several tail carbon atoms in both phases are given in Table 6 together with data from neutron diffraction experiments (Zaccai et al. 1979). The positions are averaged over both tails in order to compare with the experimental data. Taking into account the experimental error, the mean positions in both phases compare well with experiment. The deviation in the C_{15} positions is substantial, but the experimental data for this position are not realistic as C_{14} and C_{15} positions differ by more than a bond length. In the theoretical model of Meraldi and Schlitter (1981), neutron diffraction data can be reproduced except for the C_{15} position, just as in our simulations. The agreement with Wiener and White (1992a) is much better: these authors find a width of 0.5 nm for the terminal methyl. MD and experimental distribution half widths in the L_α phase are of the same order of magnitude and increase both towards the middle of the bilayer. In the L_β phase the MD distribution half widths show the opposite tendency, and are also twice as large as the experimental data. Obviously, in the MD gel phase the molecules as a whole have large mutual displacements along the bilayer normal which is, among other reasons, caused by the inhomogeneity of the MD system. The MD results for methylene groups in the palmitoyl tails indicate that C_2 (below the carbonyl C) in tail 1 is more deeply buried in the hydrocarbon region than C_2 in tail 2. The difference is 0.1 nm in the L_α phase and 0.1 to 0.2 nm in the L_β phase. DMR (Seelig and Seelig 1975, 1980) and neutron diffraction values (Zaccai et al. 1979) confirm this shift. It is explained by the observation that tail 1 starts from the glycerol backbone parallel with the bilayer normal whereas tail 2 is initially kinked away from this orientation.

Charge distributions

We calculated time-averaged charge distributions along the bilayer normal for choline, phosphate, and carboxy ester groups, and for water molecules. The distributions were obtained by subdividing the unit cell into slices along the bilayer normal, and assigning for each coordinate frame every (partial) atomic charge to the slice it resides in. Integration of these distributions to reduce the noise resulted in cumulative charge distributions which are given in Figs. 7 and 8 for the L_α and L_β phases, respectively. Since the choline and phosphate atom distributions overlap to a large extent, their charge group distributions largely cancel. For dipole orientations perpendicular to the bilayer normal and for very diffuse interfaces the headgroup charge distribution would vanish completely. This is indeed the case in the L_β phase where the charge accumulation is less than in the L_α phase in spite of the full physical charges in this phase. The remaining cumulative charge is almost completely neutralized in both phases by the distribution of the water molecules, just as in our previous simulations (Egberts 1988; Egberts and Berendsen 1988). This is exactly what we expect from a medium with a high dielectric constant. As is shown in subsequent work (Marrink et al. 1993), the charge compensation due to the ordering of the water dipole is of direct importance to the decay of the hydration force between lipid bilayers.

Density profile

From X-ray experiments it is in principle possible to evaluate the electron density profile in a membrane. We calculated the time-averaged z-distributions of electrons in both simulations, which can be evaluated with good accuracy, as all atomic positions are known. In Fig. 9 a comparison is presented for the L_α phase between MD and experimental electron density with conditions close to the MD run (Levine and Wilkins 1971). The only reported profile for the L_β phase does not permit a meaningful comparison as it applies to mitochondria lipids. The two profiles have the same shape: a minimum in the middle of the bilayer (near the CH_3 groups), a maximum at the position of the headgroups, and a local minimum in the

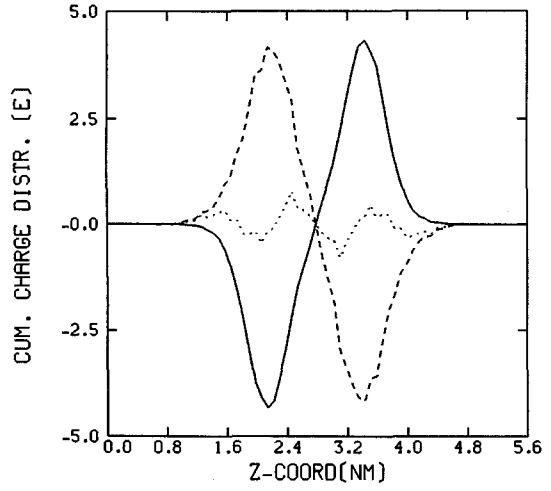

Fig. 7. Cumulative charge distributions along bilayer normal of water (*dashed line*), phosphate + choline groups (*solid line*), and total membrane (*dotted line*) in the L_α phase. The z-coordinate runs as in Fig. 5

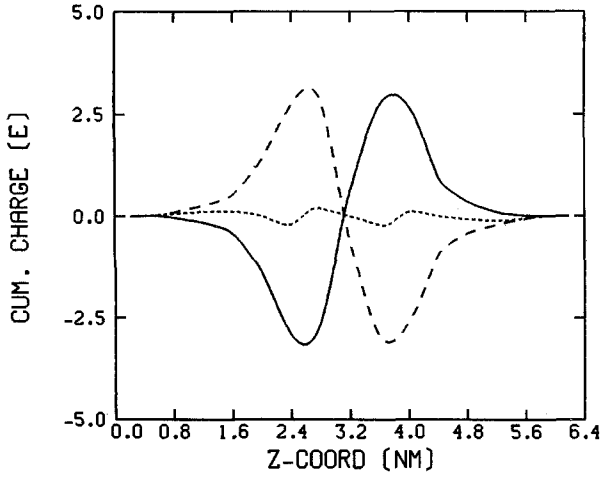

Fig. 8. Cumulative charge distributions along bilayer normal of water (*dashed line*), phosphate + choline groups (*solid line*), and total membrane (*dotted line*) in the L_β phase. The z-coordinate runs as in Fig. 6

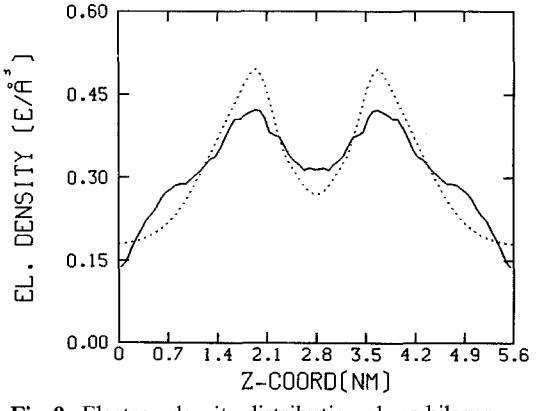

Fig. 9. Electron density distribution along bilayer normal in the L_α phase. MD (*solid line*) and experimental (dotted line; Levine and Wilkins 1971) results. The z-coordinate runs as in Fig. 5

water layer. Obviously, the headgroups are closely packed owing to the favorable dipole-dipole interactions between them. Towards the middle of the bilayer the number of gauche angles increases since the gauche angle is stabilized in the neighbourhood of end groups. In addition, methyl groups pack with a lower density than methylene groups do. An increase in free volume results, as is also shown by the statistical mechanical calculations of Gruen (1981).

We also calculated the mass density distribution across the membrane which shows the same shape as the electron density distribution, as expected. It turns out that the mass density at the beginning of the lipid tails is 1.10 g/cm^3. This density resembles the mass density of several soft polymers (0.9–1.3 g/cm^3). At carbon position 9 the density has dropped to the density of liquid hexadecane (0.753 g/cm^3). In the middle of the bilayer the density is significantly lower, dropping to 0.60 g/cm^3. From this it can be concluded that the hydrocarbon interior of the membrane in the liquid crystalline phase is far from homogeneous.

Hydrocarbon chain conformations and flexibility

The fractions of trans angles per tail in the L_α phase are 0.73 and 0.74 in tail 1 and tail 2, respectively. In the L_β phase these values are 0.88 and 0.89. The difference between the tails is statistically insignificant. The number of gauche angles per tail (n_g) is 3.5 in the L_α and 1.5 in the L_β phase. Experimental results for the L_α phase are: 3.6–4.2 from IR spectroscopy (Mendelsohn et al. 1989), 4.3 from DMR (Seelig and Seelig 1974, 1980), and 5.2 from Raman measurements (Pink et al. 1980). For the L_β phase $n_g = 1.2$ has been derived (Pink et al. 1980). Theoretical predictions for n_g in the L_α phase are: 4.0 (Meraldi and Schlitter 1981), 3.9 (Gruen 1981), and 3.1 (Marsh 1974). The L_α simulation compares well with theoretical predictions, but experimental values are somewhat higher.

The fraction of trans dihedral angles does not vary significantly along the palmitoyl chains. Only the dihedrals at the tail ends have a larger fraction gauche angles, since the rotation barrier is lower near the end of the tails. This was also observed experimentally (Mendelsohn et al. 1989). In both phases a single gauche rotation or two gauche rotations of like sign for $\gamma_1 - \gamma_5$ (glycerol linkage to tail 1) are frequently observed. This can be interpreted as an attempt to line up the tails with the bilayer normal. Initially they run in the direction dictated by the glycerol backbone, which is at an angle of $\pm 45°$ with the bilayer normal. The beginning of tail 2 ($\beta_1 - \beta_3$) is characterized by a frequently observed kink ($g^+ tg^-$ or $g^- tg^+$ configuration) in order to achieve a lateral separation between the two tails.

The distribution of kinks over the other dihedral angles does not vary along the chains either. We calculated 0.58 kinks per chain in the L_α phase and 0.14 in the L_β phase. Dilatometric measurements (Träuble and Haynes 1974) have been interpreted to give 0.6 and 0.1, respectively. Theoretical predictions for the L_α phase are: 0.6 (Schindler and Seelig 1975), 0.5 (Meraldi and Schlitter

1981) and 0.2 (Marsh 1974). From a random distribution of gauche angles, excluding g^+g^- and g^-g^+, and using the fraction trans angles in the simulation, we obtain for the number of kinks per chain: 0.26 in the L_α phase and 0.06 in the L_β phase. The actual number of kinks is at least twice as large, and the distribution of gauche angles over the chains is therefore non random. In the lipids in the previous simulation (Egberts 1988; Egberts and Berendsen 1988) with C_{10} chain length this effect was not observed. This is in good agreement with the tendency observed in simulations by Edholm (private communications), that longer chains show an increase in the fraction of kinks. In addition, we now deal with two hydrocarbon chains per lipid. Steric repulsion and hydrophobic aggregation of the two tails require lateral displacements of the chains, and these are most easily accommodated by means of kinks. Dihedral transitions in the tails were monitored during the simulation. In both simulations and for both tails they occur two to three times as frequently near the tail ends as near the glycerol backbone. In the L_α phase the time between two transitions of the same dihedral angle is on average 19.8 ps for tail 1, and 20.3 ps for tail 2. In the L_β phase the values are 29.5 and 31.0 ps, respectively. The two tails thus behave equivalently in both phases, being more flexible in the liquid-crystalline phase. No experimental results are known for the dihedral transition rates.

Life times of kinks were calculated from a fit of the kink autocorrelation function to a single exponential decay. In the L_α phase the mean kink life time is 7.3 ps, in the L_β phase 3.4 ps. The disturbance caused by a kink, the parallel displacement of a chain, it more easily accomodated in the L_α phase, with its higher surface area per tail.

Figure 10, finally, gives projected structures of representative conformations of DPPC molecules in the L_α and L_β phase, obtained from snapshots in both runs.

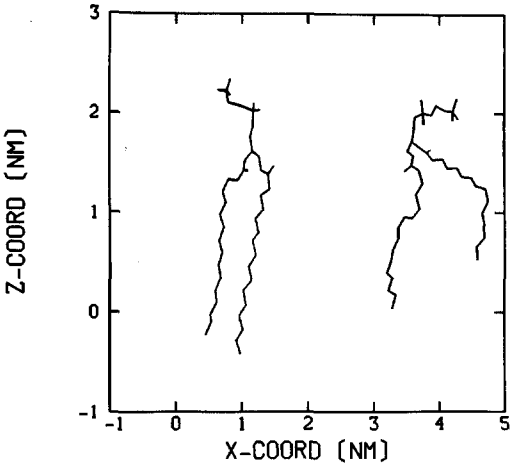

Fig. 10. Two-dimensional representation of a typical conformation of a DPPC molecule as found in the L_α (*right*), and in the L_β phase (*left*)

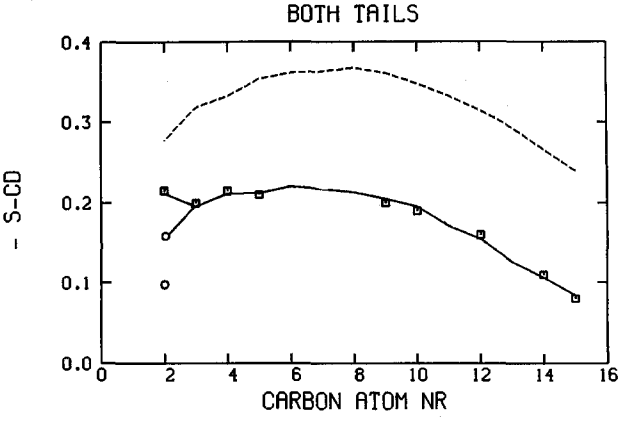

Fig. 11. Order parameters $-S_{CD}$ as a function of carbon atom number in the palmitoyl tails in the L_α phase (*dotted line*), in the L_β phase (*dashed line*), and from DMR experiments on the L_α phase (squares; Seelig and Seelig 1974, 1980). All values are averaged over both tails, except for carbon atom number 2 (below the carbonyl C) where the lower line (MD) and the circles (DMR) are the values for tail two

Hydrocarbon chain order parameters

A useful way to compare the chain configurations found by MD with experiments is by means of their order parameters. The formal definition of the order parameter tensor S is:

$$S_{ij} = \frac{1}{2}\langle 3 \cos \Theta_i \cos \Theta_j - \delta_{ij} \rangle \qquad (1)$$

in which Θ_i represents the angle between the i^{th} molecular axis and the bilayer normal (z-axis). The brackets denote an ensemble average. Molecular axes are defined per CH_2 unit. For the n^{th} CH_2 unit these are:

z: vector from C_{n-1} to C_{n+1},
y: vector $\perp$ to z and in the plane through C_{n-1}, C_n, and C_{n+1},
x: vector $\perp$ to z and y.

An S_{zz} that equals 1 indicates full order along the bilayer normal, $-1/2$ full order perpendicular to the normal, and 0 an isotropic distribution.

A frequently used and non-perturbing method to determine the order in acyl chains of lecithin molecules is deuterium NMR on selectively deuterated compounds. This method yields an order parameter S_{CD} that is defined for the direction along the C–D bond and can be directly related to the MD order parameters through the expression: $S_{CD} = 2/3\ S_{xx} + 1/3\ S_{yy}$.

In Fig. 11 we give MD order parameters $-S_{CD}$ for both phases and order parameters from DMR in the L_α phase at 50 °C (Seelig and Seelig 1974, 1980). Agreement in the L_α phase is excellent. Spin label data (Horvath et al. 1980), as well as DMR data for DMPC (Meier et al. 1986) suggest order parameters that almost double on going from the L_α to the gel phase, in qualitative agreement with our findings. In both phases a plateau is observed extending approximately over the first 10 carbons. The larger fraction of gauche angles at the tail ends results in a more isotropic distribution of the last carbon atoms, reflected in order parameters approaching 0. The DMR results on DPPC specifically deuterated at the C_2 position show that the two carbon atoms are physically inequivalent. For tail 2 two values of $-S_{CD}$ are observed.

These have been assigned to slightly different average orientations of the two C–D vectors. Our value for tail 2 is an average value which coincides with the highest experimental value.

Headgroup orientation

In order to reveal the orientation of the headgroups, we calculated the angular distributions around the bilayer normal of the lecithin dipole vectors in both phases. In Fig. 12 the distributions $f(\Theta)\sin\Theta$ are displayed, where Θ is the angle between the dipole vector and the bilayer normal. The dipole vectors tend to be inclined relative to the bilayer plane, this tendency being more pronounced in the L_β phase. The average angle of the dipole vector with the bilayer normal is 59° in the L_α phase, and 70° in the L_β phase. From the atom distributions we calculated the average z-component of the P–N distance, i.e. its projection onto the bilayer normal, to be 0.2 nm in the L_α phase and 0.11 nm in the L_β phase. These values already point to an inclination of the dipoles towards the bilayer plane and support the present calculation.

Experimental evidence (Seelig 1978) suggests dipole orientations almost perpendicular to the bilayer normal in both the liquid-crystalline and the gel phase. This is a preferable conformation from an electrostatic point of view. However, the MD results show a preference for a small angular deviation from the bilayer plane. We presume that a more coplanar arrangement of the dipoles is disfavored by the steric hindrance of the bulky headgroups, and by the tendency of the choline group to dissolve into the water layer. A larger surface area per lipid headgroup is disfavoured by the attraction between the tails. In the MD L_β phase a more coplanar arrangement can be realized because of the larger spread of the molecules along the bilayer normal, despite the higher surface density.

Headgroup conformations and flexibility

We will discuss headgroup conformations in terms of the state of the dihedral angles. The fraction trans and gauche angles of the headgroup dihedrals in the two phases are presented in Table 7.

MD results for α_5 show a large fraction of gauche dihedral angles: 57% in the L_α phase and 75% in the L_β phase. This ties in neatly with various experimental (X-ray (Sundaralingam 1972; Hauser et al. 1981), DMR (Seelig 1978), Raman and PMR (Akutsu 1981) results for α_5 which all point to a predominant fraction of gauche angles. The α_4 dihedral is preferentially trans, both in the L_α phase (72%) and in the L_β phase (84%), in good agreement with X-ray results (Sundaralingam 1972; Hauser et al. 1981) and Raman measurements (Akutsu 1981). A quantitative analysis of NMR results (London et al. 1979) yields a fraction trans in the L_α phase between 65 and 75%. Quantum chemical and statistical calculations (Frischleder 1980; Frischleder and Peinel 1982) on phospholipids also point to an $\alpha_3-\alpha_5\ t\,g^{\pm}$ conformation.

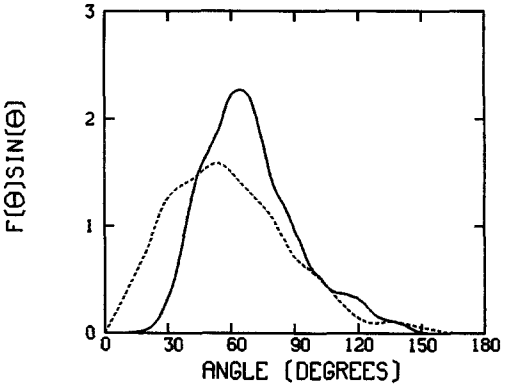

Fig. 12. Angular distributions with respect to the bilayer normal of lecithin dipole vectors in the L_α phase (*dashed*) and L_β phase (*solid line*)

Table 7. Fraction of trans and gauche angles of headgroup dihedrals

	L_α			L_β		
	g^-	t	g^+	g^-	t	g^+
Θ_1	0.175	0.455	0.370	0.345	0.320	0.335
α_1	0.155	0.700	0.145	0.070	0.845	0.085
α_2	0.345	0.255	0.400	0.325	0.300	0.375
α_3	0.305	0.270	0.425	0.325	0.335	0.340
α_4	0.140	0.720	0.140	0.105	0.835	0.060
α_5	0.255	0.430	0.315	0.400	0.255	0.345

The α_2 and α_3 dihedrals are primarily found in the g^+g^+ or g^-g^- sequence, in full accord with what is generally assumed. The α_1 dihedral is 70% trans in the L_α phase and 85% trans in the L_β phase. From X-ray diffraction (Seelig and Gally 1976; Hauser et al. 1981) α_1 is trans. Theoretical models (London et al. 1979; Frischleder 1980) also predict a large fraction of trans dihedral angles for α_1.

The rotation around glycerol C_2-C_3 (Θ_1) is not restricted very much. Trans and gauche states are equally populated in the L_β phase, the trans state is slightly preferred in the L_α phase. NMR results (Akutsu and Kyogoku 1977; Seelig 1977) indicate a rotation of the lecithin group as a whole around the C_2-C_3 bond of the glycerol backbone. X-ray measurements (Hauser et al. 1981; Sundaralingam 1972) as well as theoretical calculations (Frischleder 1980; Frischleder and Peinel 1982) also reveal both trans and gauche torsion angles Θ_1.

So far, only the isomerism of single dihedrals has been examined. The spectrum of dihedral combinations of Θ_1, $\alpha_1-\alpha_5$ in the simulations is very broad. In contrast, the dihedral angles of the glycerol backbone have a few preferred conformations. The four most stable conformations for angles $\Theta_1-\Theta_4$ are $t\,g^+\,t\,g^-$, $g^+\,g^-\,t\,g^-$, $g^-\,t\,t\,g^-$, and $t\,g^+\,g^-\,g^+$ in both phases. They cover 88.5% in the L_α phase and 93% in the L_β phase of the total spectrum. It is apparent that the glycerol backbone is more rigid than the headgroup. Especially the $t\,g^-$ sequence for $\Theta_3-\Theta_4$ forms a major stabilizing factor. From an analysis of dihedral transitions it is found that the transition rate of these

two angles is also lower than that of the other dihedrals. The $t\,g^-$ sequence implies that palmitoyl tail 1 runs off in the direction of the glycerol backbone, whereas tail 2 is initially parallel to the bilayer plane. Separation of the two tails to avoid steric hindrance therefore accounts for the observed stability of the $t\,g^-$ sequence for $\Theta_3-\Theta_4$.

The only data available for dihedral sequences come from X-ray data. Crystal data, however, can only partly account for conformations in the gel and liquid-crystalline phases. In general the sequences found in the crystalline phase are 'carried' over to the L_α and L_β phase, but also some other conformations show up with high probability.

In order to investigate the flexibility of the choline group we calculated the order parameters S_{CD} of its CH_2 segments and the order parameter S_{zz} of the CH_2-N vector. Values in the L_α phases are: -0.03 and -0.01 for S_{CD} and 0.05 for S_{zz}. The MD values in the L_β phase are not qualitatively different from these values. This demonstrates that there is no significant restriction on the movement of the $N(CH_3)_3$ group and the choline methyl segments in both phases. The CH_2-N vector has no fixed orientation with respect to the bilayer and undergoes rapid oscillations of large amplitude. Experiments (Gally et al. 1975; Tamm and Seelig 1983) show the same trend. Values are reported for S_{CD} of the choline methyl groups of approximately -0.04, and for S_{zz} of the CH_2-N vector between 0.07 and 0.17.

The order parameter S_{zz} of the glycerol C_2-C_3 vector is 0.31 in the L_α phase and 0.48 in the L_β phase. Seelig and Gally (1976) derived a value of 0.66 from the experimental value (Seelig et al. 1977; Brown et al. 1979; Seelig 1978) of S_{CD} (-0.22) for glycerol C_3, assuming isotropic rotation around the C_2-C_3 bond, leading to $S_{zz}=-3\,S_{CD}$. We calculate values for S_{CD} of glycerol C_3 of -0.15 (L_α phase) and -0.25 (L_β phase), implying $S_{zz}=-2\,S_{CD}$. We therefore conclude that it is not likely that isotropic rotation around the C_2-C_3 bond exists.

Diffusion constants

Lateral diffusion constants D of lecithin molecules were calculated from mean squared displacements r in two dimensions (x, y) of the centers of mass of the molecules, using the formula:

$$\lim_{t\to\infty} \langle r^2(t)\rangle = 4\,D\,t \qquad (2)$$

In Table 8 we give the values of the lateral diffusion constants of lecithin, together with the range of experimental values as determined by Pulsed NMR (Rubinstein et al. 1979; Lindblom and Wennerström 1977), Fluorescence Recovery After Photobleaching (Smith and McConnell 1978; Wu et al. 1977; Vaz et al. 1987; Fahey and Webb 1978; Sheats and McConnell 1978) and spin-label experiments (McConnell et al. 1971). Since experiments on diffusion are often determined at temperatures close to the phase transition temperature, 315 K, we also included the reduced values of the MD diffusion constants at 325 K for the L_α phase and at 310 K for the L_β phase. Experimental

Table 8. Lateral diffusion constants (cm^2/s) of lipids

MD, L_α	MD_{RED}, L_α	EXP, L_α	MD, L_β	MD_{RED}, L_β	EXP, L_β
$5.1\cdot0^{-6}$	$2.5\cdot10^{-6}$	10^{-7}–10^{-8}	$7.1\cdot10^{-7}$	$3.6\cdot10^{-7}$	10^{-10}

results (Vaz et al. 1987) indicate that in this region the diffusion constant approximately doubles every 25 K.

Though it is clear from the experimental values that the determination of D is not unambiguous, most of the reported experimental values are smaller than the MD values by at least one order of magnitude in the L_α phase and three orders of magnitude in the L_β phase. However, since the diffusion of lipids is such a slow process, it might well be that the total simulation time is insufficient to determine the long time diffusion constant. In that case the calculated diffusion constants represent the diffusion of the lipids in the potential well of their neighbours, which is much faster. Evaluation of the mean displacement of the lipid molecules, which turned out to be one neighbour distance, indicated that this is indeed the case. The discrepancy with the L_β phase is also related to the incomplete gel state attained in the simulation, leaving liquid-crystalline patches with fast diffusion.

Diffusion constants of water molecules and their dependence on position along the bilayer normal will be described elsewhere (Marrink and Berendsen, to be published).

Conclusions

Our simulations of a phospholipid bilayer in the liquid-crystalline state yield a very detailed picture on a microscopic level of static arrangement and dynamic properties of the constituent molecules. This picture is in good agreement with experimental results obtained on equivalent natural and synthetic membranes. The system that we defined can serve as a starting point for extended simulations incorporating other molecules (peptides, proteins or lipid mixtures) or to study phase transitions and transport phenomena. The simulations have already been extended to study the permeation of water through the membrane. (Marink and Berendsen, to be published) and to study hydration force between membranes (Marrink et al. 1993).

The MD results for the gel phase of this membrane must be interpreted with due caution, because the full hexagonal order expected for the gel phase could not develop in the simulation. However, the simulations do give insight in the changes that occur at the main phase transition.

Finally we would like to stress that the textbook picture of statically, homogeneously aggregated lipids, serving merely as an operation field for the proteins, should be replaced by a more dynamical, inhomogeneous one in which the membrane has a role of its own. Not only our work, but also other simulations and various experiments over the last few years have shown that a biological membrane is more complex than usually assumed.

Acknowledgements. This work was supported by the Foundation for Biophysics, under the auspices of the Netherlands Organization for Scientific Research, NWO.

References

Akutsu H (1981) Direct determination by raman scattering of the conformation of the choline group in phospholipid bilayers. Biochemistry 20:7359–7366

Akutsu H, Kyogoku Y (1977) Conformational difference in the polar groups of phosphatidylcholine and phosphatidylethanolamine in aqueous phase. Chem Phys Lipids 18:285–303

Bareman JP, Klein ML (1990) Collective tilt behavior in dense, substrate-supported monolayers of long-chain molecules: a molecular dynamics study. J Phys Chem 94:5202–5205

Berendsen HJC, Postma JPM, Gunsteren WF van, Hermans J (1981) Interaction models for water in relation to protein hydration. In: Pullman B (ed) Intermolecular forces. Reidel, Dordrecht, pp 331–342

Berendsen HJC, Postma JPM, Gunsteren WF van, Dinola A, Haak JR (1984) Molecular dynamics with coupling to an external bath. J Chem Phys 81:3684–3690

Braganza LF, Worcester DL (1986) Hydrostatic pressure induces hydrocarbon chain interdigitation in single-component phospholipid bilayers. Biochemistry 25:2591–2596

Brown MF, Seelig J, Häberlen U (1979) Structural dynamics in phospholipid bilayers from deuterium spin-lattice relaxation time measurements. J Chem Phys 70:5045–5053

Büldt G, Gally HU, Seelig A, Seelig J, Zaccai G (1978) Neutron diffraction studies on selectively deuterated phospholipid bilayers. Nature 271:182–184

Büldt G, Gally HU, Seelig J (1979) Neutron diffraction studies on phosphatidylcholine model membranes. J Mol Biol 134:673–691

Cevc G (1987) How membrane chain melting properties are regulated by the polar surface of the lipid bilayer. Biochemistry 26:6305–6310

Chandrasekhar I (1992) In: Gaber BP, Easwaran KRK (eds) Biomembrane structure and function. Adenine Press, New York, p 353

Chapman D, Williams RW, Ladbrooke BD (1967) Physical studies of phospholipids. VI. Thermotropic and lyotropic mesomorphism of some 1,2-diacylphosphatidylcholines (lecithins). Chem Phys Lipids 1:445–475

Egberts E (1988) Molecular dynamics simulation of multibilayer membranes. Ph.D.Thesis, Rijksuniversiteit Groningen

Egberts E, Berendsen HJC (1988) Molecular dynamics simulation of a smectic liquid crystal with atomic detail. J Chem Phys 89:3718–3732

Fahey PF, Webb WW (1978) Lateral diffusion in phospholipid bilayer membranes and multilamellar liquid crystals. Biochemistry 17:3046–3053

Frischleder H (1980) Quantum-chemical and empirical calculations on phospholipids. VII The conformational behavior of the phosphatidylcholine headgroup in layer systems. Chem Phys Lipids 27:83–92

Frischleder H, Peinel G (1982) Quantum-chemical and statistical calculations on phospholipids. Chem Phys Lipids 30:121–158

Gally HU, Niederberger W, Seelig J (1975) Conformation and motion of the choline head group in bilayers of dipalmitoyl-e-sn-phosphatidylcholine. Biochemistry 14:3647–3652

Gruen DWR (1981) A mean-field model of the alkane-saturated lipid bilayer above the phase transition. I. Development of the model. Biophys J 33:149–166

Gunsteren WF van, Berendsen HJC (1977) Algorithms for macromolecular dynamics and constraint dynamics. Mol Phys 34:1311–1327

Gunsteren WF van, Berendsen HJC (1987) Groningen molecular simulation (GROMOS) library manual, Biomos, Nijenborgh 4, 9747 AG Groningen, The Netherlands

Hauser H, Pascher I, Pearson RH, Sundell S (1981) Preferred conformation and molecular packing of phosphatidylethanolamine and phosphatidylcholine. Biochim Biophys Acta 650:21–51

Hockney RW, Eastwood JW (1981) Computer simulation using particles. McGraw-Hill, New York

Horvath LI, Cirak J, Vigh L (1980) Relation of raman order parameters to spin labeling parameters. Chem Phys Lipids 27:237–250

Inoko Y, Mitsui T (1978) Structural parameters of dipalmitoyl phosphatidylcholine lamellar phases and bilayer phase transitions. J Phys Soc Japan 44:1918–1924

Janiak MJ, Small DM, Shipley GG (1976) Nature of the thermal pretransiton of synthetic phospholipids: dimyristoyl- and dipalmitoyllecithin. Biochemistry 15:4575–4580

Janiak MJ, Small DM, Shipley GG (1979) Temperature and compositional dependence of the structure of hydrated dimyristoyl lecithin. J Biol Chem 254:6068–6078

Jönsson B, Edholm O, Teleman O (1986) Molecular dynamics simulations of a sodium octanoate micelle in aqueous solution. J Chem Phys 85:2259–2271

Levine YK, Wilkins MHF (1971) Structure of oriented lipid bilayers. Nature New Biol 230:69–72

Lewis BA, Engelman DM (1983) Lipid bilayer thickness varies linearly with acyl chain length in fluid phosphatidylcholine vesicles. J Mol Biol 166:211–217

Lewis RNAH, Mannock DA, McElhaney RN (1989) Effect of fatty acyl chain length and structure on the lamellar gel to liquid-crystalline and lamellar to reversed hexagonal phase transitions of aqueous phosphatidylethanolamine dispersions. Biochemistry 28:541–548

Lindblom G, Wennerström H (1977) Biological and model membranes studies by nuclear magnetic resonance of spin one half nuclei. Q Rev Biophys 10:67–96

Lis LJ, McAlister M, Fuller N, Rand RP, Parsegian VA (1982) Interactions between neutral phospholipid bilayer membranes. Biophys J 37:657–665

London RE, Walker TE, Wilson DM, Matwiyoff NA (1979) Application of doubly decoupled carbon-13{proton, nitrogen-14}-NMR spectroscopy to studies of phospholipids. Chem Phys Lipids 25:7–14

Loof H de, Harvey SC, Segrest JP, Pastor RW (1991) Mean field stochastic boundary molecular dynamics simulation of a phospholipid in a membrane. Biochemistry 30:2099–2113

Marrink SJ, Berkowitz M, Berendsen HJC (1993) Molecular dynamics simulation of a membrane/water interface: the ordering of water and its relation to the hydration force. Langmuir (in press)

Marsh D (1974) Statistical mechanics of the fluidity of phospholipid bilayers and membranes. J Membr Biol 18:145–162

McConnell HM, Devaux P, Scandella C (1971) In: Fox CF (ed) Membrane research. Academic Press, New York

Meier P, Ohmes E, Kothe G (1986) Multipulse dynamic nuclear magnetic resonance of phospholipid membranes. J Chem Phys 85:3598–3614

Mendelsohn R, Davies MA, Brauner JW, Schuster HF, Dluhy RA (1989) Quantitative determination of conformational disorder in the acyl chains of phospholipid bilayers by infrared spectroscopy. Biochemistry 28:8934–8939

Meraldi JP, Schlitter J (1981) A statistical mechanical treatment of fatty acyl chain order in phospholipid bilayers and correlation with experimental data. B. Dipalmitoyl-3-sn-phosphatidylcholine. Biochim Biophys Acta 645:193–210

Moller MA, Tildesley DJ, Kim KS, Quirke N (1991) Molecular dynamics simulation of a Langmuir-Blodgett film. J Chem Phys 94:8390–8401

Nagle JF, Wiener MC (1988) Structure of fully hydrated bilayer dispersions. Biochim Biophys Acta 942:1–10

Phillips MC, Williams RM, Chapman D (1968) Hydrocarbon chain motions in lipid liquid crystals. Chem Phys Lipids 3:234–244

Pink DA, Green TJ, Chapman D (1980) Raman scattering in bilayers of saturated phosphatidylcholines. Experiment and theory. Biochemistry 19:349–356

Ploeg P van der, Berendsen HJC (1982) Molecular dynamics simulation of a bilayer membrane. J Chem Phys 76:3271–3276

Ploeg P van der, Berendsen HJC (1983) Molecular dynamics of a bilayer membrane. Mol Phys 49:233–248

Reiss-Husson J (1967) Structure des phases liquide-cristallines de différents phospholipides, monoglycérides, sphingolipides, anhydres ou en présence d'eau. J Mol Biol 25:363–382

Rubinstein JLR, Smith BA, McConnell HM (1979) Lateral diffusion in binary mixtures of cholesterol and phosphatidylcholines. Proc Natl Acad Sci, USA 76:15–18

Ruocco MJ, Shipley GG (1982) Characterization of the sub-transition of hydrated dipalmitoylphosphatidylcholine bilayers. Biochim Biophys Acta 691:309–320

Ryckaert JP, Bellemans A (1975) Molecular dynamics of liquid n-butane near its boiling point. Chem Phys Lett 30:123–125

Ryckaert JP, Bellemans A (1978) Faraday Discuss Chem. Soc. 66:95

Ryckaert JP, Ciccotti G, Berendsen HJC (1977) Numerical integration of the cartesian equations of motion of a system with constraints: Molecular dynamics of *n*-alkanes. J Comp Phys 23:327–341

Schindler H, Seelig J (1975) Deuterium order parameters in relation to thermodynamic properties of a phospholipid bilayer. A statistical mechanical interpretation. Biochemistry 14:2283–2278

Seelig J (1977) Deuterium magnetic resonance: theory and application to lipid membranes. Q Rev Biophys 10:353–418

Seelig J (1978) Nuclear magnetic resonance and the head group structure of phospholipids in membranes. Biochim Biophys Acta 515:105–140

Seelig J, Gally HU (1976) Investigation of phosphatidylethanolamine bilayers by deuterium and phosphorus-31 nuclear magnetic resonance. Biochemistry 15:5199–5204

Seelig A, Seelig J (1974) The dynamic structure of fatty acyl chains in a phospholipid bilayer measured by deuterium magnetic resonance. Biochemistry 13:4839–4845

Seelig A, Seelig J (1975) Bilayers of dipalmitoyl-3-sn-phosphatidylcholine conformational differences between the fatty acyl chains. Biochim Biophys Acta 406:1–5

Seelig J, Seelig A (1980) Lipid conformation in model membranes and biological membranes. Q Rev Biophys 13:19–61

Seelig J, Gally HU, Wohlgemuth R (1977) Orientation and flexibility of the choline head group in phosphatidylcholine bilayers. Biochim Biophys Acta 467:109–119

Sheats JR, McConnell HM (1978) A photochemical technique for measuring lateral diffusion of spin-labeled phospholipids in membranes. Proc Natl Acad Sci, USA 75:4661–4663

Smith BA, McConnell HM (1978) Determination of molecular motion in membranes using periodic pattern photobleaching. Proc Natl Acad Sci, USA 15:2759–2763

Sundaralingam M (1972) Molecular structures and conformations of the phospholipids and sphingomyelins. Ann NY Acad Sci, USA 195:324–355

Tamm LK, Seelig J (1983) Lipid solvation of cytochrome c oxidase. Deuterium, nitrogen-14, and phosphorus-31 nuclear magnetic resonance studies on the phosphocholine head group and on cis-unsaturated fatty acyl chains. Biochemistry 22:1474–1483

Tardieu A, Luzzati V, Reman FC (1973) Structure and polymorphism of the hydrocarbon chains of lipids: a study of lecithin-water phases. J Mol Biol 75:711–733

Tenchov BG, Lis LJ, Quinn PJ (1987) Mechanism and kinetics of the subtransition in hydrated L-lipalmitoylphosphatidylcholine. Biochim Biophys Acta 897:143–151

Träuble H, Haynes DH (1974) Volume change in lipid bilayer lamellae at the crystalline-liquid crystalline phase transition. Chem Phys Lipids 7:324

Ulmius J, Wennerström H, Lindblom G, Arvidson G (1977) Deuteron nuclear magnetic resonance studies of phase equilibria in a lecithin-water system. Biochemistry 16:5742–5745

Vaz WLC, Stümpel J, Hallmann D, Gambacorta A, Rosa M de (1987) Bounding fluid viscosity and translational diffusion in a fluid lipid bilayer. Eur Biophys J 15:111–115

Wiener MC, White SH (1992a) Structure of a fluid dioleoylphosphatidylcholine bilayer determined by joint refinement of x-ray and neutron diffraction data. II. Distribution and packing of terminal methyl groups. Biophys J 61:428–433

Wiener MC, White SH (1992b) Structure of a fluid dioleoylphosphatidylcholine bilayer determined by joint refinement of x-ray and neutron diffraction data. I. Complete structure. Biophys J 61:434

Wu E, Jacobson K, Papahadjopoulos D (1977) Lateral diffusion in phospholipid multibilayers measured by fluorescence recovery after photobleaching. Biochemistry 16:3936–3941

Zaccai G, Büldt G, Seelig A, Seelig J (1979) Neutron diffraction studies on phosphatidylcholine model membranes. II Chain conformation and segmental disorder. J Mol Biol 134:693–706

Zaccai G, Blasie JK, Schoenborn BP (1980) Neutron diffraction studies on the location of water in lecithin bilayer model membranes. Proc Natl Acad Sci, USA 72:376–380